Biosensors and Bioelectronics 34 (2012) 261–266

Contents lists available at SciVerse ScienceDirect

Biosensors and Bioelectronics

journal homepage: www.elsevier.com/locate/bios

A molecular machine biosensor: Construction, predictive models and experimental studies

Sahar Moradi-Monfared [a], Vikram Krishnamurthy [a,*], Bruce Cornell [b]

[a] Department of Electrical and Computer Engineering, University of British Columbia, 5500 - 2332 Main Mall, Vancouver, BC, V6 T 1Z4, Canada
[b] Surgical Diagnostics Ltd., St Leonards, NSW 2065, Australia

ARTICLE INFO

Article history:
Received 29 November 2011
Received in revised form 3 February 2012
Accepted 10 February 2012
Available online 19 February 2012

Keywords:
Chemically modified electrode
Ion channel biosensor
Molecular detection
Surface based chemical reactions
Fluid flow dynamics
Compartment modeling

ABSTRACT

This paper describes the construction, operation and predictive modeling of a molecular machine, functioning as a high sensitivity biosensor. Embedded gramicidin A (gA) ionchannels in a self-assembled tethered lipid bilayer act as biological switches in response to target molecules and provide a signal amplification mechanism that results in high sensitivity molecular detection. The biosensor can be used as a rapid and sensitive point of care diagnostic device in different media such as human serum, plasma and whole blood without the need for pre and post processing steps required in an enzyme-linked immunosorbent assay. The electrical reader of the device provides the added advantage of objective measurement. Novel ideas in the construction of the molecular machine, including fabrication of biochip arrays, and experimental studies of its ability to detect analyte molecules over a wide range of concentrations are presented. Remarkably, despite the complexity of the device, it is shown that the response can be predicted by modeling the analyte fluid flow and surface chemical reactions. The derived predictive models for the sensing dynamics also facilitate determining important variables in the design of a molecular machine such as the ion channel lifetime and diffusion dynamics within the bilayer lipid membrane as well as the bio-molecular interaction rate constants.

1. Introduction

Advances in micro-fluidics and transduction technologies have led to the development of biosensors capable of bimolecular detection at very low concentrations of analyte (e.g. femto molar) without the need to label the participating molecules (Barroso et al., 2011; Bayley and Cremer, 2001; Separovic and Cornell, 2007). This paper presents the novel engineering and biochemistry involved in the construction, modeling and experimental results of such a biosensor, whose transduction mechanism uses ion channels. Many researchers have explored modulating the ionic current of ion channels to engineer molecular detection mechanisms (Bayley and Cremer, 2001; Separovic and Cornell, 2007). The approach used in the molecular machine studied here, whilst using ion channel transduction provides a mechanism that may be engineered to target many different classes of molecules by custom designing antibody receptors. The molecular machine we consider comprises gramicidin A (gA) ion channels connected to a receptor group via a linker and embedded in a lipid bilayer tethered to a gold electrode by a disulphide bond. The device is very sensitive and is capable of detecting target molecular species at concentrations less than 1pM (Cornell et al., 1997; Cornell, 2002; Separovic and Cornell 2007). The functionality of the device depends on a supramolecular tethered membrane assembly of approximately 1000 × 1000 lipids with a single ion channel modulating the flow of millions of ions per second in a sensing event of typically 5 min. The three dimensional binding of analyte to the sensing surface receptors causes a change in the membrane conductance, proportional to the concentration of the analye molecules in the sample solution. Other approaches to biosensor design based on synthetic lipid monolayers and bilayers have been reported by several groups (Bayley and Cremer, 2001; Peterman et al., 2002).

In previous work, a preliminary version of the biosensor studied here, was used along with electrical impedance spectroscopy to study dynamics of small transmembrane peptides in the lipid bilayer (Suzuki et al., 2007; Yin et al., 2003). Compared to (Yin et al. 2003), as described below we provide new experimental results and detailed mathematical models for the sensing dynamics that yield accurate predictions of the response of the ion channel molecular sensor under various operating conditions. In (Krishnamurthy et al., 2010b), preliminary results are presented on the reaction rate modeling of the biosensor.

How can the sensing dynamics of the biosensor be modeled? Despite the complexity of the device, this paper presents

* Corresponding author. Tel.: +1 604 822 2653; fax: +1 604 822 5949.
E-mail addresses: smonfare@ece.ubc.ca (S. Moradi-Monfared), vikramk@ece.ubc.ca (V. Krishnamurthy), brucec@surgicaldiagnostics.com (B. Cornell).

0956-5663/$ – see front matter © 2012 Elsevier B.V. All rights reserved.
doi:10.1016/j.bios.2012.02.018

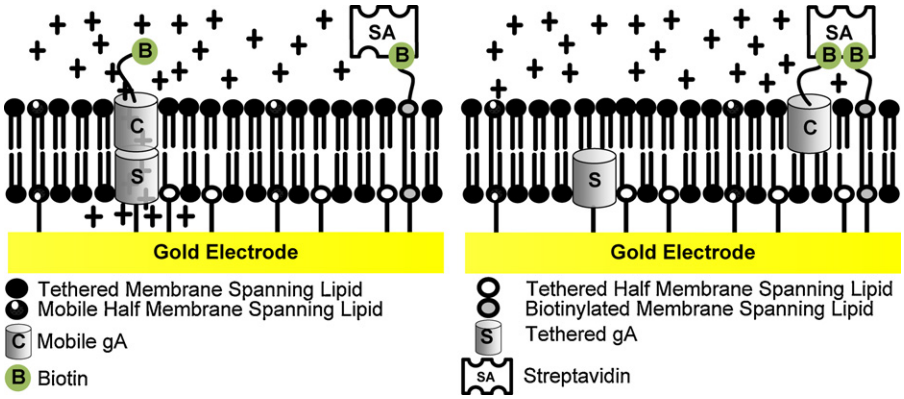

Fig. 1. Construct used in the detection of streptavidin (sa) when biotin is used as the receptor molecule. Binding of streptavidin to the biotin immobilized on the gold electrode and attached to the free moving gA monomer, *c*, causes the free moving gA monomer to become immobilized. This in turn prohibits the formation of conductive dimer, *d*.

mathematical models that accurately predict the response of the biosensor over a wide range of analyte concentrations. Such predictive models require a description of the advection and diffusion of analyte molecules in the fluid flowing adjacent to the detection surface as well as the chemical interactions at the electrode surface (Squires et al., 2008). This is done here through the use of an advection diffusion partial differential equation (PDE) coupled to a non-linear system of ordinary differential equations. Similar models are used to model sandwich assays in lateral flow bio-reactors and the BIACORE surface plasmon resonance (SPR) optical system (Myszka et al., 1998; Qian and Bau, 2003). Under mass transport limited conditions a depletion zone forms close to the electrode surface. The dynamics of the depletion zone is modeled here by a two-compartment model (Katiyar et al., 2010; Squires et al., 2008)

The predictive models developed are exploited to optimise the response of the biosensor when the flow rate, receptor density and reaction rates are modified. The predictive models are also used to estimate bio-chemical interaction rates of elements within the device including ion channel lifetimes and diffusion dynamics within the bilayer lipid membrane as well as the bio-molecular interaction rate constants. As will be described below, the estimates obtained are close to that obtained in experimental studies in the literature. The predictive models also provide useful insight into the qualitative behavior of the biosensor; depending on the Damkohler number, the biosensor response can be classified into reaction rate limited or mass transport limited.

2. Results

In this section, we highlight novel features involved in the construction, operation and modeling of the gA ion channel biosensor. The validity of the models is verified by comparing the experimental response of the biosensor with its predicted response.

2.1. Ion channel sensor operation and construction

As shown in Fig. 1, the inner layer of the bilayer lipid membrane contains four tethered species: tethered gA molecules, (*s*), membrane spanning lipids (MSLs), biotinylated membrane spanning lipids (BMSLs), (*b*), and half membrane spanning lipids (HMSL). The bilayer is formed by the addition of mobile non-tethered species which are added after the tethered species have been chemically adsorbed to the gold electrode. The mobile species are a mix of two chain bulky headgroup amphiphile, diphytanyl ether phosphatidylcholine (DPEPC) and a two chain small headgroup amphiphile, glycero diphytanyl ether (GDPE). The ratio of these mobile amphiphiles is adjusted to achieve the best membrane seal yielding the lowest conduction in the absence of the outer layer mobile ion channels. Since gramicidin has a terminal ethanolamine group which permits a range of chemistries, the biosensor may be prepared for use with a wide range of receptors to detect many different analytes.

How does the biosensor detect analyte molecules? The BMSL span the bilayer membrane, and extend into the outer bathing solution providing a binding site for receptor groups, or as shown in Fig. 1, for streptavidin–biotin gating which is used here as a demonstration of the generic gating mechanism of the biosensor. The outer lipid layer also contains untethered biotinylated gA monomers, (*c*), with biotin linked via a 5-aminocaproyl linker to the gA (gA5XB). This complex is also free to move laterally within the two dimensional plane of the BLM. When two non-conducting monomers in the upper (*c*) and lower lipid layers (*s*) align to form a dimer, (*d*), the dimerised gA ion channels become conductive. The arrival of analyte (*a*) cross-links receptors (biotin in the demonstration) attached to the mobile outer layer gA monomers to those attached to BMSL. Due to the low density of tethered gA channels within the inner membrane layer, this anchors them distant, on average, from their mobile outer layer partners. Gramicidin dimerisation is thus prevented and the conductance decreases. Applying a small alternating potential between the gold substrate and a reference electrode in the test solution generates a charge at the gold surface which causes electrons to flow in an external circuit (Cornell et al., 1997; Cornell, 2002; Separovic and Cornell, 2007). This is a key element in this device and any measuring technique that couples electronic flow in a wire into a physiological solution of ions. The results of a clinical study involving detection of influenza A virus in different types of respiratory specimens using the biosensor studied here are reported in Appendix A of the Supporting Information. The sensitivity and specificity of the biosensor are proven by comparing the results against the results obtained by culture.

The streptavidin–biotin interaction is one of the best characterised bio-molecular interactions ever reported and provides an excellent case study for the purpose of verifying the derived mathematical models. The detection mechanism in the device may of course be adapted to target any antigenic species for which a suitable receptor is attached at the sites occupied here by Biotin. An example of this may easily be demonstrated by attaching biotinylated antibody fragments (b-Fab) to the streptavidin–biotin complex shown in Fig. 1. This now elicits the same response as seen on the addition of streptavidin to a membrane with just Biotin, but now the response is only observed when the analyte targeted by the Fab is added. The magnitude and speed of the response may be estimated from replacing streptavidin–biotin reaction rates with the binding constants of the analyte and Fab using the model described here.

Table 1
Typical parameter values for streptavidin–biotin interaction. These parameters determine the dynamics of the sensing response of the molecular machine.

Primary species concentration	Analyte A (pM)	1–1000
	Mobile gA monomers C* (molecules/cm^2)	1×10^9
	Tethered gA monomers S* (molecules/cm^2)	1×10^{10}
	Tethered binding site B* (molecules/cm^2)	1×10^9
Reaction rate constant	$f_1 = f_2 = f_6$(M/s)	8×10^6
	$f_3 =$ f_4 (cm^2 molecules s)	5×10^{-9}
	$f_5 =$ f_7 (cm^2 molecules s)	1×10^{-10}
	$r_1 = r_2 = r_3 = r_4 = r_6$(s^{-1})	1×10^{-6}
	$r_5 = r_7$ (s^{-1})	1.5×10^{-2}
Chamber dimensions	h (mm)	0.1
	W (mm)	3
	L (mm)	0.7
Diffusivity constant	γ (cm^{2}s)	1.5×10^{-6}
Flow rate	Q (μL min)	100
Mass transport coefficient	k_M (cm s)	0.0018
Diffusion layer thickness	δ	6.8041 μm
Damkohler number	D_a	0.1771

The speed and sensitivity of the response of the biosensor is directly proportional to the number of binding sites accessible to each free gA monomer in the upper lipid layer. The diffusion of the free gA molecules allows an individual untethered gA monomer to access many potential analyte capture sites at the tethered BMSL binding sites. This results in an amplification of the apparent rate of mobile gA channels cross-linking with the BMSL sites in the ratio of the number of BMSL sites to the number of free gA molecules. This results in a significantly faster response and a greater sensitivity. However as the density of the BMSL capture sites, B, is increased streptavidin depletion develops at the electrode surface and sample flow must be introduced to correct this sample depletion. For this purpose the biosensor assembly includes a micro-fluidic chamber with a rectangular cross section of dimensions height, h, width, W, and length, L. Typical dimensions are given in Table 1.

2.2. Predictive models for biosensor response

This section shows that reaction rate models coupled with fluid flow dynamics provide accurate predictions of the biosensor response over a wide range of analyte concentrations. The response rate is determined by the transport of analyte molecules to the sensing surface, the reaction rates of the analyte molecule with its receptor at the electrode surface, the two dimensional diffusion rates and cross-linking reaction rates in the plane of the membrane surface.

The kinetics of the chemical reactions induced at the biosensor electrode due to the introduction of analyte are described by the system of non-linear differential equations denoted in Eq. (1), where $u = [B, C, D, S, W, X, Y, Z]^T$ is a vector containing the concentrations of the primary species as well as the complexes that are formed at the electrode according to the reactions in Eq. (2).

$$\frac{du}{dt} = Mr(u) \tag{1}$$

$$a + b \underset{r_1}{\overset{f_1}{\Leftrightarrow}} w \quad a + c \underset{r_2}{\overset{f_2}{\Leftrightarrow}} x \quad w + c \underset{r_3}{\overset{f_3}{\Leftrightarrow}} y \quad x + b \underset{r_4}{\overset{f_4}{\Leftrightarrow}} y$$

$$c + s \underset{r_5}{\overset{f_5}{\Leftrightarrow}} d \quad a + d \underset{r_6}{\overset{f_6}{\Leftrightarrow}} z \quad x + s \underset{r_7}{\overset{f_7}{\Leftrightarrow}} z \tag{2}$$

In Eq. (2), f_i and r_i are the three and two dimensional intrinsic forward and backward reaction rate constants, respectively. The rapid diffusion of untethered gA monomers, c, in the outer lipid layer is described in the two dimensional reaction rate constants. The interaction of the analyte molecules with the binding sites are described by the three dimensional rates. In Eq. (1), $r(u) = [R_1, R_2, \ldots, R_7]^T$ with T indicating transpose of a vector, R_i indicating the rate of the i^{th} reaction in Eq. (2) (e.g. $R_1 = f_1AB - r_1W$) and M denoting the stoichiometry matrix. The initial conditions are described in Appendix B of the Supporting Information.

The analyte concentration in the flow chamber is modeled by the advection diffusion partial differential equation in Eq. (3). subject to the boundary conditions denoted in Eq. (4)(a)–(d). Cartesian coordinates are introduced, with x_1 axis along the direction of flow and x_3 perpendicular to the direction of flow.

$$\frac{\partial A}{\partial t} = \gamma \left(\frac{\partial^2 A}{\partial x_1^2} + \frac{\partial^2 A}{\partial x_3^2} \right) - v(x_3) \frac{\partial A}{\partial x_1} \tag{3}$$

$$A(x_1 = 0, x_3, t > 0) = A^* \quad \text{(a)}$$

$$\frac{\partial A}{\partial x_1}(x_1 = L, x_3, t > 0) = 0 \quad \text{(b)} \tag{4}$$

$$\frac{\partial A}{\partial x_3}(x_1, x_3 = h, t > 0) = 0 \quad \text{(c)}$$

$$\gamma \frac{\partial A}{\partial x_1}(x_1, x_3 = 0, t > 0) = \psi(t) \quad \text{(d)}$$

In the above equations t denotes time, $A(x_1, x_3, t)$ denotes the analyte concentration, A^* denotes the analyte injection concentration, γ is the analyte diffusivity and $v(x_3)$ describes the fully developed velocity profile in the flow chamber.

Boundary condition at $x_1 = L$ Eq. 4(b), states that the exit flux of analyte is due entirely to convective flow and not diffusion. This approximation is justified in the Supporting Information Appendix C.

In Eq. (4)(d), $\psi(t)$ gives the rate by which analyte molecules are grabbed by immobilized species at the electrode surface and can be found from the reactions in Eq. (2) to be

$$\psi(t) = -A(f_1B + f_2C + f_6D) + r_1W + r_2X + r_6Z \tag{5}$$

When mass transport and surface reaction rates are comparable the advection diffusion model, defined by Eq. (3), Eqs. (4) and (5) is numerically solved to obtain the system response.

2.3. Predictive models under reaction rate limited and mass transport limited conditions

Depending on the relative influence of mass transport effects to surface chemical reactions, it is possible to accurately approximate the advection diffusion partial differential equation (Eq. (3)) by simpler predictive models involving ordinary differential equations (He et al., 2006; Myszka et al., 1998; Squires et al., 2008). Such an approximation can then be used to estimate the analyte concentration A^*. The relative influence of mass transport effects and surface chemical reactions is determined by the Damkohler number, D_a, which is the ratio of the reactive flux to the diffusive flux (Tang et al., 2004). It is defined by $D_a = (f_1 h\theta)/\gamma$, where $\theta = B^* + C^*$ is the total concentration of the binding sites (Squires et al., 2008). B^* and C^* denote the initial concentration of the primary species, b and c, values of which are reported in Table 1.

Under reaction rate limited conditions, $D_a > 100$, analyte concentration at the electrode surface, $A_s = A^*$, and the flow dynamics are decoupled from the surface chemical reactions (Tang et al. 2004). In this region the well mixed model (WMM), defined by the system of non-linear ordinary differential equations in Eq. (1), with $A = A^*$, describes the system dynamics accurately.

Under mass transport influenced conditions, i.e., $D_a > 100$ or $100 > D_a > 0.01$, as analyte molecules are scavenged by the surface species, a depletion zone of thickness, δ, is created close to the electrode surface (Tang et al., 2004). The emergence of the depletion zone makes it possible to approximate the advection diffusion partial differential equation by a simplified predictive model known as the two compartment model (TCM) (Myszka et al., 1998). The two compartment model, adapted to our biosensor is denoted by

$$\begin{aligned} h_i \frac{dA(t, x_3 < h_i)}{dt} &= \psi(t) + k_M(A^* - A) \quad x_3 \le h_i \\ A(t, x_3 > h_i) &= A^* \qquad\qquad\qquad\quad x_3 \le h_i \end{aligned} \tag{6}$$

where h_i denotes the height of the inner compartment and is $\sim\delta$. k_M is the rate constant that characterises the diffusion of analyte molecules between the inner and the outer compartments and is estimated by $k_M \approx 1.282\,(\gamma^2\bar{v}/hL)^{1/3}$ (Katiyar et al., 2010; Myszka et al., 1998). The maximum height of the inner compartment, i.e. δ, can be estimated using non-dimensional flow parameters as discussed in Appendix D of the Supporting Information. The value of δ is shown in Table 1.

2.4. Comparison of predicted and experimental responses

Two measures are used here to report on the change in membrane conductance in response to the introduction of analyte molecules. They are the gating magnitude, $GM = |(G_{final} - G_{initial})|/G_{initial}$ and the normalized maximum slope, *NMS*, which is the maximum slope of the kinetic response normalized by the initial dimer concentration, $D(0)$. Fig. 2 shows the normalized experimental and predicted biosensor responses to 1000 pM, 100 pM, and 10 pM challenges of streptavidin when the primary species concentrations are set to values given in Table 1.

Percentage differences between the predicted and experimental GM and NMS values for streptavidin concentrations of 1000 pM, 100 pM, 10 pM and 10 pM are shown in Fig. 3.

The Damkohler number, D_a, for this system, for the streptavidin–biotin interaction, is calculated to be, $D_a = 0.1771$. The system is therefore more reaction rate limited than diffusion limited. However, as seen from Fig. 3, although predictions from the advection diffusion PDE and the two compartment model are very similar to the experimental values of GM and NMS, predictions from the well mixed model, except for the 1 nM concentration, are the least accurate and deteriorate as the target concentration is decreased. This is due to the increased influence of mass transport effects for lower analyte concentrations (see Appendix E in the Supporting Information). The same increase in mass transport effects is observed when binding site density is increased.

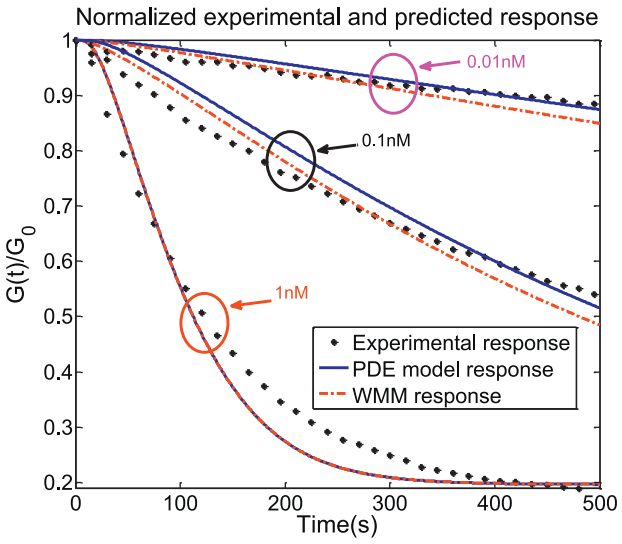

Fig. 2. Experimental and predicted response to 1000 pM, 100 pM, and 10 pM challenges of streptavidin when biotin is used as the receptor molecule. WMM denotes the well mixed model. PDE is used to denote the advection diffusion partial differential equation, while TCM is used to denote the two compartment model.

The response of the sensor to various concentrations of ferritin is also included in Appendix G in the Supporting Information. In this set up streptavidin is used as a coupling protein. The binding site and the free moving gA monomers have biotinylated linker arms and these are coupled through streptavidin, to biotinylated antibodies.

3. Discussion

This section explores multi-analyte detection capability by fabricating biochip arrays. Also, the predictive models derived in the previous sections, are used to obtain the detection limits of the device.

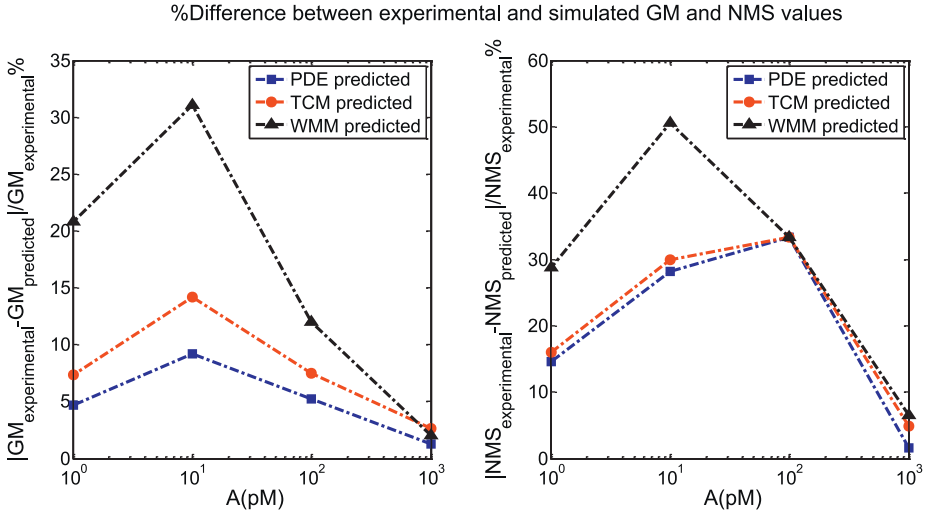

Fig. 3. Difference between predicted and experimental gating magnitude GM, and normalized maximum slope, NMS, values as percentage of the experimental values. It can be seen that when the well mixed model (WMM) is used, the difference between the experimental and predicted values increases as the analyte concentration is decreased. The advection diffusion (PDE) and the two compartment models (TCM) on the other hand produce accurate *GM* and *NMS* predictions compared to the experimental values.

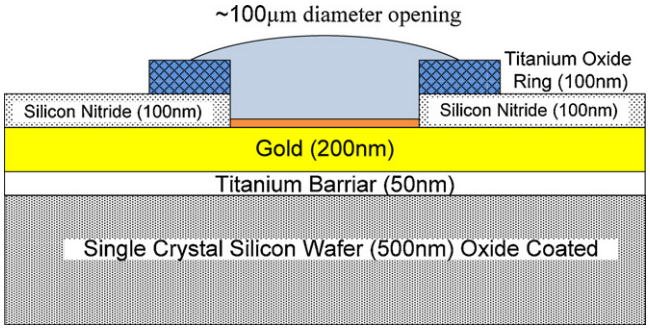

Fig. 4. Cross section of one element in a silicon chip sensor array. The design incorporates five layers: (i) an underlying silicon wafer, (ii) a 50 nm titanium (Ti) barrier, (iii) a 200 nm gold layer, (iv) a 100 nm silicon nitride (Si_3N_4) layer and a patterned ring of titanium oxide (TiO_2). The titanium oxide ring is designed to provide a hydrophilic surface at the membrane edge.

3.1. Biochip arrays

By constructing arrays of biosensors fabricated using silicon nitride, silicon carbide and glass substrates, multi-analyte detection capability is achieved. Multi-analyte detection is an advantage as it permits on board calibration to correct for systematic variations which can occur across an electrode array and to correct for electrode to electrode variation between different sensors. In fact as discussed in (Krishnamurthy et al., 2010a) reproducibility of the results is substantially improved by incorporating a calibrator channel. A novel element in the design of these arrays is the use of a titanium oxide ring at the perimeter of the electrode opening. The titanium ring is designed to provide a mechanical seal for the outer leaflet preventing it from diffusing beyond the area of the tethered inner leaflet lipids. In addition, the titanium seal retains water during the patterning of antibodies, and during the dry down process for storage. A schematic of the design of an element in a silicon chip is shown in Fig. 4.

3.2. Rate constants, gramicidin dimer lifetime and diffusion

The response kinetics of the biosensor can be used to extract reaction rate constants between the participating analyte and receptor molecules. In this paper, the biomolecular interaction is that of streptavidin and biotin which is determined here as possessing an association rate constant $f_1 = 8 \times 10^6\,M^{-1}s^{-1}$ and a dissociation rate constant $r_1 = 10^{-6}(1/s)$. These values are comparable to those reported by others (Srisa-Art et al., 2008).

Using the predictive models, it is estimated here that the gramicidin dimer lifetime is 70(s). The estimated value of dimer lifetime is comparable to the average gA dimer lifetime measured in a solvent free phosphatidylcholine membranes in (Sawyer et al., 1990), similar to the one used here. Using the derived dynamical models the diffusion rate of the free moving gA monomers in the outer lipid layer, c, is also determined to be $f_3 = 5 \times 10^{-9}\,(cm^2\ molecules\ s)$. The association rate of the free moving gA monomer, c, and the tethered gA monomer, s, is determined to be $f_5 = 10^{-10}\,(cm^2\ molecules\ s)$.

3.3. Biosensor design improvement using the predictive models

Factors that influence the biosensor response are the flow rate, Q, the analyte concentration, A, the binding site density, B, the free moving gA monomer concentration, C, and the tethered gA monomer concentration, S (Krishnamurthy et al., 2010b). When the molecular machine is used as a biosensor, the limiting detection threshold is defined as the minimum analyte concentration that produces a signal that can be differentiated from the background signal by 2–3 standard deviations. Here we use the derived dynamical models to explore the improvements in sensor performance (GM and NMS) as the total binding site density, θ and flow rate, Q, are increased.

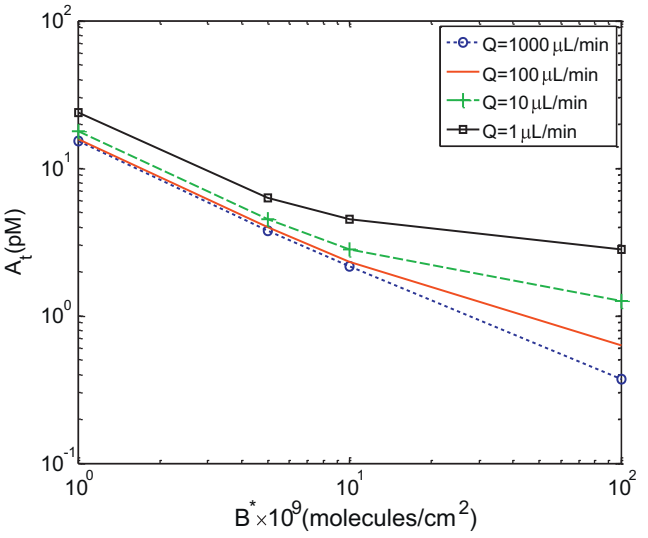

Fig. 5. Improvement in the biosensor limiting detection threshold, A_t, as the binding site density, B^*, and flow rate, Q, are increased. Liming detection threshold, A_t, is defined as the minimum analyte concentration that causes a 10% decrease in the gating magnitude GM.

Based on the existing responses we have taken a 10% decrease in GM as a reference for a detectable signal. Fig. 5 shows the minimum streptavidin concentrations, A_t, that produce a 10% decrease in GM in 5 min, as the binding site density (Biotin density) is increased for $Q = [1, 10, 100, 1000](\mu L\,min)$. As the binding site density, B^* increases the sensitivity increases, i.e., A_t decreases.

As the binding site density is increased the normalized maximum slope of the biosensor response also increases. Appendix F in the Supporting Information contains a discussion about the improvement in NMS for $A^* = [1, 10, 100, 1000](pM)$ at $B^* = 10^9$ molecules cm^2 as the binding site density and flow rate is increased.

3.4. Effect of flow rate

The predictive models can be used to achieve design specific optimization of flow rate. For example for the streptavidin–biotin interaction Fig. 5 shows that to achieve $A_t = 16$ pM on a chip where $B^* = 10^9$ molecules/cm^2, a flow rate of at least 100 μL min is required. Fig. 5 shows that as an increase in binding site density improves the sensitivity of the device, so does an increase in Q. The effectiveness of Q in increasing the sensitivity of the device increases with greater binding site density and lower analyte concentration, A. However it should be noted that for any specific chip design (i.e., binding site density), once the flow rate is increased to overcome the mass transfer effects then the A_t will reach a limiting value depending on B^*. A very similar effect is seen for the normalized maximum slope. As discussed in Appendix F a 10-fold increase in the flow rate significantly improves the NMS value for lower anlayte concentrations (i.e., $A^* = 1$ pM)) at larger binding site densities. Since at lower anlayte concentrations and higher binding site densities the reactive flux is larger compared to the diffusive flux which results in increased mass transport effects. Thus increasing the flow rate reduces these effects and improves the system response.

4. Conclusion

This paper has described the construction and operation of a novel ion channel based sensing machine. Novel dynamical models were derived to predict the response of the device. By using these models, we can obtain performance limits on the biosensor. For example we have shown that a 10% response is achieved in 5 min at streptavidin concentration $A_t = 16$ pM when $\theta = 2 \times 10^9$ molecules cm^2 and that this performance requires a sample flow rate of $Q = 100\,\mu$L min to overcome analyte depletion effects caused by the high capture density. The mathematical models show that higher binding site densities and higher sample flow rates improve this detection limit although not linearly. The derived models were also used to infer important bio-molecular interaction constants, such as the streptavidin–biotin on and off rates of $f_1 = 8 \times 10^6\,\mathrm{M}^{-1}\,\mathrm{s}^{-1}$ and $r_1 = 10^{-6}(1/\mathrm{s})$ respectively, the gA dimer lifetime of 70(s), dimer formation rate of $f_5 = 10^{-10}\,(\mathrm{cm}^2\,\text{molecules s})$ and free moving gA monomer diffusion rate of $f_3 = 5 \times 10^{-9}\,(\mathrm{cm}^2\,\text{molecules s})$ in the lipid layer. These values compare well with values obtained previously under similar circumstances.

5. Materials and methods

The gold electrode is made by evaporating 100 nm, 99.9995% gold (5n5 gold) film onto specially molded 25 mm × 75 mm polycarbonate slides. The inner tethered lipid layer is formed by exposing the slide to an ethanol solution containing 370 μM total of the tethered species, including tethered gA monomers ($370/10^4$ μM), the MSL ($370/10^2$ μM), the half membrane spanning lipids 70($3/1.1$ μM) and the biotinylated BMSL ($370/10^3$ μM) for 30 min. The outer layer is formed by rinsing the slide in alcohol and then exposing it for 2 min to a second ethanol solution containing the mobile, half membrane spanning lipids (70:30 DPEPC:GDPE) 3 mM total concentration and the biotinylated gA5XB (15 nM). The lipid bilayer forms spontaneously after rinsing with phosphate buffered saline (PBS). Streptavidin solutions were prepared by dilution in PBS from streptomycine avidities lyophilized powder purchased from SIGMA (CAT number 85878-1MG).

Appendix A. Supplementary data

Supplementary data associated with this article can be found, in the online version, at doi:10.1016/j.bios.2012.02.018.

References

Barroso, M.F., de-los Santos-Ivarez, N., Delerue-Matos, C., Oliveira, M., 2011. Biosens. Bioelectron. 30, 1–12.
Bayley, H., Cremer, P., 2001. Nature 413, 226–230.
Cornell, B., 2002. In: Ligler, F., Taitt, C. (Eds.), Optical Biosensors: Present and Future. Elsevier, Amsterdam, p. 457.
Cornell, B., Braach-Maksvytis, V., King, L., Osman, P., Raguse, B., Wieczorek, L., Pace, R., 1997. Nature 387, 580–583.
He, X., Coombs, D., Myszka, D., Goldstein, B., 2006. Bull. Math. Biol. 68, 1125–1150.
Katiyar, A., Thiel, S., Guliants, V., Pinto, N., 2010. J. Chromatogr. A 1217, 1583–1588.
Krishnamurthy, V., Monfared, S., Cornell, B., 2010a. IEEE Trans. Nanotechnol. 9, 303–312.
Krishnamurthy, V., Monfared, S., Cornell, B., 2010b. IEEE Trans. Nanotechnol. 9, 313–321.
Myszka, D., Xiaoyi, H., Micah, D., Morton, T., Goldstein, B., 1998. Biophys. J. 75, 583–594.
Peterman, M., Ziebarth, J., Braha, O., Bayley, H., Fishman, H., Bloom, D., 2002. Biomed. Microdevices 4, 231–236.
Qian, S., Bau, H., 2003. Anal. Biochem. 322, 89–98.
Sawyer, D., Oiki, S., Anderson, O., 1990. Biophys. J. 57, A100.
Separovic, F., Cornell, B., 2007. In: Chung, S., Andersen, O., Krishnamurthy, V. (Eds.), Biological Membrane Ion Channels. Springer-Verlag, New York, pp. 595–621.
Squires, T., Messinger, R., Manalis, S., 2008. Nat. Biotechnol. 26, 417–426.
Srisa-Art, M., Dyson, E., deMello, A., Edel, J., 2008. Anal. Chem. 80, 7063–7067.
Suzuki, H., Tabata, K.V., Noji, H., Takeuchi, S., 2007. Biosens. Bioelectron. 22, 1111–1115.
Tang, L., Kwon, H., Kang, K., 2004. Biotechnol. Bioeng. 88, 869–879.
Yin, P., Burns, C., Osman, P., Cornell, B., 2003. Biosens. Bioelectron. 18, 389–397.